AN ABSTRACT OF THE THESIS OF

Patrick U. Volz for the degree of Master of Science in Electrical and Computer Engineering presented on May 5, 1995. Title: Decentralized Control of a Cable-Stayed Beam Structure.

Abstract approved: _____

Mario E. Magaña

In this thesis the active reduction of the vertical vibration of a cable-stayed beam structure due to an external excitation using a decentralized control strategy is studied. The beam structure chosen represents the left-end girder of a cable-stayed bridge and the external load considered is that of an earthquake. Control forces are exerted through actuators that are attached at the anchorages of the stay cables and change the cable length based on velocity information of collocated sensors. Therefore the resulting controllers are of low dimension and no information has to be transmitted along the beam structure. The decentralized controllers are designed using a finite-dimensional lumped-mass model of the beam structure and the performance of the controlled system is demonstrated by computer simulations. Both a pole placement method and an optimal control method are used for the controller design.

Decentralized Control of a Cable-Stayed Beam Structure

by

Patrick U. Volz

A THESIS

submitted to

Oregon State University

in partial fulfillment of
the requirements for the
degree of

Master of Science

Completed May 5, 1995
Commencement June 1995

Master of Science thesis of Patrick U. Volz presented on May 5, 1995

APPROVED:

Redacted for Privacy

Major Professor, representing Electrical and Computer Engineering

Redacted for Privacy

Chair of Department of Electrical and Computer Engineering

Redacted for Privacy

Dean of Graduate School

I understand that my thesis will become part of the permanent collection of Oregon State University libraries. My signature below authorizes release of my thesis to any reader upon request.

Redacted for Privacy

Patrick U. Volz, Author

Dedicated to Melanie

Acknowledgments

I would like to thank everybody who assisted and supported me during the preparation of this work. Especially I would like to thank my parents. Their support made it possible for me to come to Oregon State University.

Table of Contents

List of Figures

List of Symbols

Symbol	Description
$\mathbf{A}$	system matrix
$\mathbf{A}_i$	system matrix of i-th subsystem
$\mathbf{A}_{ij}$	interconnection matrix between i-th and j-th subsystem
$A_{2,4}$	cross-sectional area of left and right stay cable
$a_Q(t)$	external disturbance (earthquake acceleration)
$\mathbf{B}$	control input matrix
$\underline{b}_{2,4}$	control input vector of subsystem 2 and 4
$\mathbf{C}$	damping matrix of closed-loop system
$c_{2,4}$	damping coefficient of subsystem 2 and 4
$\mathbf{D}$	symmetric square root of $\mathbf{Q}$; $\mathbf{DD}^T = \mathbf{Q}$
D_i	arbitrary constants (in Appendix A)
d	distance between lumped masses
E	modulus of elasticity of beam
$E_{2,4}$	modulus of elasticity of left and right stay cable
$\underline{E}_i$	influence vector of external disturbance of i-th subsystem
e_i	influence constant of external disturbance of i-th subsystem
F	vertical point static force
$\underline{F}(t)$	vector of forces at location of lumped masses
$F_i(t)$	force applied at the location of the i-th lumped mass

List of Symbols (Continued)

Symbol	Description
$\underline{F}_C(t)$	vector of control forces on lumped masses
$\underline{F}_C^*(t)$	modal vector of control forces
$F_{C2,4}(t)$	force due to left and right stay cable
$\underline{F}_Q(t)$	vector of forces on lumped masses due to external disturbance
$\underline{F}_Q^*(t)$	modal vector of forces due to external disturbance
$\underline{F}_S$	vector of gravitational forces of lumped masses
$f_{2,4}$	velocity feedback gain of left and right actuator
$\underline{G}$	optimal control gain vector
$\underline{G}_{2,4}$	optimal control gain vector of subsystem 2 and 4
g	gravitational acceleration
$\mathbf{H}_i$	constant, symmetric, and positive definite matrices
H_i	arbitrary constants (in mode shape functions)
I	moment of inertia of beam
$I_{2,4}$	control influence constant of left and right actuator
$\mathbf{K}$	stiffness matrix of beam model
$\mathbf{K}^*$	stiffness matrix of beam model including stiffness constants of stay cables
$\Delta K_{2,4}$	stiffness constant of left and right stay cable
k_i	modal stiffness of i-th mode
L	length of beam

List of Symbols (Continued)

Symbol	Description
$L_{2,4}$	length of left and right stay cable
$\mathbf{M}$	mass matrix of beam model
m	mass per unit length of beam
m_B	mass of beam
m_L	mass of lump
$\bar{\mathbf{P}}$	solution to algebraic Ricatti equation
$\mathbf{Q}$	state weighting matrix
$\mathbf{Q}_{2,4}$	state weighting matrix of subsystem 2 and 4
$\mathbf{R}$	control weighting matrix
$r_{2,4}$	control weight of subsystem 2 and 4
$\mathbf{S}_i$	constant, symmetric, and positive definite matrices
$\underline{s}(t)$	state variables of system
$\underline{s}_i(t)$	state variables of i-th subsystem
t	time
$\underline{u}(t)$	control input of system
$\underline{u}^*(t)$	optimal control input of system
$u_{2,4}(t)$	displacement of left and right actuator
V	performance index
$v_i(\underline{s}_i)$	norm-like function
W	a force (intermediate variable)
$\mathbf{W}$	test matrix for connective stability

List of Symbols (Continued)

Symbol	Description
w_{ij}	elements of test matrix **W**
x, x_1	spatial coordinates along the beam
$y(x,t)$	vertical beam deflection
$y_0(x)$	equilibrium deflection of beam
$\underline{y}(t)$	displacement vector of lumped masses
$\underline{y}_0$	equilibrium displacement vector of lumped masses
$y_i(t)$	vertical displacement of i-th lumped mass
$y_j(i)$	vertical displacement at the location of j-th lumped mass when a unit force is applied at the location of the i-th lumped mass
$\underline{Z}$	mode shape vector
$\underline{Z}_i$	i-th mode shape vector
$z(x,t)$	deviation from equilibrium of beam deflection
$\underline{z}(t)$	deviation from equilibrium of lumped masses
$\underline{z}^*(t)$	modal coordinates
$\beta_i(x)$	i-th mode shape function
Φ	modal transformation matrix
Γ	flexibility matrix
Λ_K	modal stiffness matrix
Λ_M	modal mass matrix
Ψ	phase angle
$\Theta_{2,4}$	angle between beam deck and left and right stay cable

List of Symbols (Continued)

Symbol	Description
$\gamma(x)$	influence function for external disturbance
$\eta_i L$	i-th solution of frequency equation of beam
λ_i	i-th eigenvalue
μ_i	i-th eigenvalue (different definition)
ω	angular frequency
ω_i	natural frequencies

DECENTRALIZED CONTROL OF A CABLE-STAYED BEAM STRUCTURE

1. Introduction

Active control of civil engineering structures, like tall buildings or long bridges is an important area of ongoing research.

A system of sensors, control units, and actuators is mounted on the structure in order to enhance its stability in the presence of external disturbances such as wind and seismic loads.

The structures are continuous or distributed parameter system which are described by partial differential equations. An exact solution to the problem of controlling a distributed system exists (1).

The dynamic response of such structures can in general be expressed in terms of modal functions and modal coordinates. Also, the response of a structure due to an external disturbance is often dominated by those system modes that are characterized by the lowest natural frequencies. Many control strategies are therefore formulated in the modal space and use linear and nonlinear feedback control, optimal control, and pole placement control strategies (2-13). One problem in this context is the estimation of the modal coordinates by means of a finite number of sensors leading to observation spillover. More problems arise if the control couples the modes of the system (8). The method of independent modal-space control (IMSC), which can be approximated by means of discrete sensors and actuators (9), preserves the independence of the individual modes and the modal control forces are calculated by means of optimal control using a quadratic performance index. In (10) the

IMSC is used to control the flutter of suspension bridges. When only a finite number of modes is considered the problem of control spillover into the uncontrolled modes (11) has to be considered. In other works, Balas studies the control of distributed systems by means of finite-dimensional controllers (12,13).

Another approach to control complex systems is decentralized control. There a system is regarded as a set of interconnected subsystems and each subsystem is controlled independently. Chen (14,15) developed a decentralized robust control strategy for uncertain complex systems. However control of all the subsystems is assumed. See (16) for an extensive treatise of decentralized control.

One specific area of application of active control of civil engineering structures are cable-stayed bridges (17). In (2,3) the feasibility of active tendon control to increase the flutter speed of a cable-stayed bridge is investigated. An active robust control scheme is used in (4) to suppress the vertical bridge vibration due to a seismic loading. An experimental study on active tendon control of cable-stayed bridges is conducted in (18). A simple cable-supported cantilever beam is used as a model and velocity feedback is used to suppress the beam vibration. The actuator and sensor are not collocated.

In this thesis the active reduction of the vertical vibration of a cable-stayed beam structure due to an external excitation using a decentralized control strategy is studied. The chosen structure represents the left-end girder of a typical cable-stayed bridge. It is supported by two stay cables. Actuators and sensors are attached at the anchorages of the stay cables. The actuators are able to change the length of the stay cables and in this way apply forces on the beam deck. The sensors measure the dynamic

response of the structure and their signals are use for feedback.

In chapter 2 a finite-dimensional model of the cable-stayed beam structure that lends itself to the application of decentralized control is introduced. The model is compared to the commonly used Euler-Bernoulli beam model and it is shown by means of a computer simulation that it gives a valid approximation of the dynamic response of the structure to an external disturbance.

In chapter 3 a decentralized control strategy that increases the stability of the beam structure against external disturbances is proposed. The stabilizing effect of the control is shown by calculation of the closed-loop eigenvalues of the system. The performance of the control strategy and also the effect of perturbations of the model are demonstrated by means of computer simulations. An outline for a theoretical proof of stability is also given. Finally, the theory of optimal control is applied to the beam model. It is demonstrated how the decentralized control strategy can be interpreted in terms of optimal control of the subsystems of the model. The decentralized result is compared to a global optimal control strategy.

The last chapter summarizes and discusses the results of this work. It also points out some of the limitations of the chosen model and areas for future research.

2. The Beam Model

In this chapter, a finite-dimensional lumped-mass model of a beam structure is developed and compared to the commonly used Euler-Bernoulli beam model.

2.1 Model Derivation

Consider the following model of a cable-stayed beam, where the beam has length L, modulus of elasticity E, moment of inertia I, and mass per unit length m. The right end of the beam is fixed, whereas the left end is simply supported.

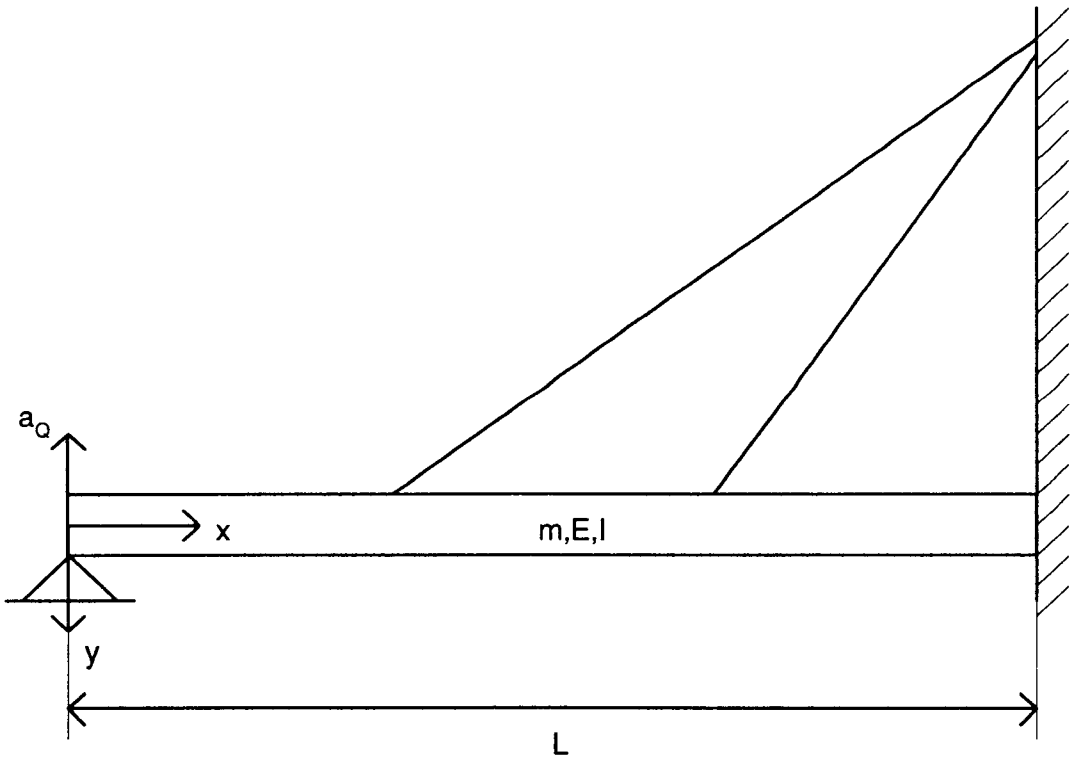

Figure 2.1 : Cable-stayed beam structure

The beam is supported by two uniform cables that are attached at one third of the beam length from each beam end.

The vertical motion y(x,t) of the beam is governed by a partial differential equation whose solution requires the knowledge of an infinite number of natural frequencies and mode shapes. Even if a finite number of modes is used to approximate the response of the system to an external load, the necessary calculations are relatively complicated.

In order to obtain a finite-dimensional model, the beam is divided into six equal sections. The masses of the sections are concentrated into lumps that are located at the section borders. The concentrated masses m_L equal one sixth[1] of the total beam mass $m_B=m \cdot L$. The distance d between the lumped masses is one sixth of the beam length L and the connecting beam is ideal and massless.

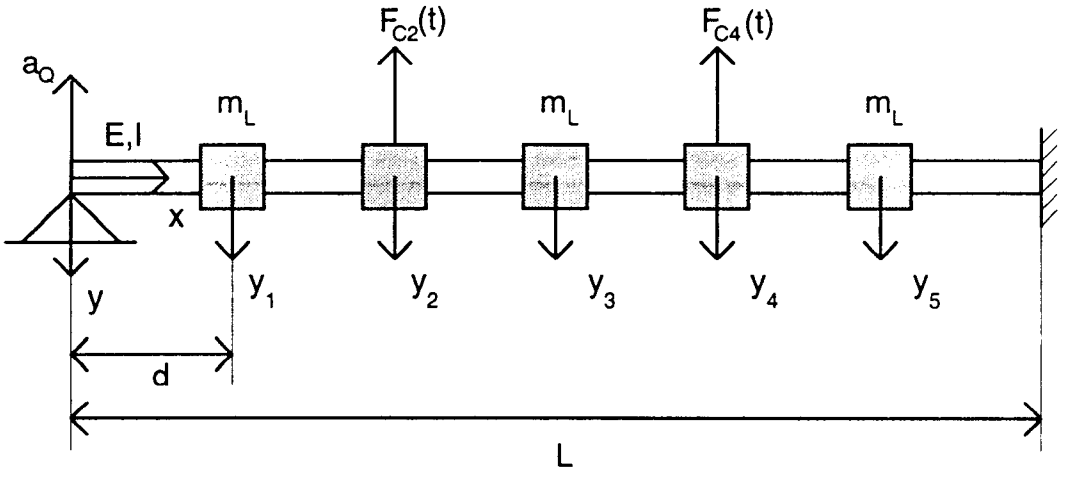

Figure 2.2 : Lumped-mass model of a cable-stayed beam

[1] One sixth of the beam mass is lumped into the beam supports and no longer contributes to the beam motion.

The vertical motion of the beam at these five locations can now be approximated by the displacements of the lumped masses y_1, y_2, y_3, y_4 and y_5, which are taken positive downward.

The number of lumped masses for this model was chosen in such a way, that the lumped masses are evenly spaced (uniform beam) along the beam and the lumped mass locations include the anchor points of the stay cables and the midspan point.

The same technique can also be applied to obtain models with a higher number of lumped masses, thus increasing the overall accuracy of the results compared to an Euler-Bernoulli beam approach. It is important, however, that the cable locations coincide with a lumped mass in order to include their effect in the equations of motion.

2.2 Equations of Motion

The equations of motion describe the dynamic behavior of the lumped masses. In order to obtain them, a relationship between forces applied at the lumped mass locations and the resulting beam displacements at these points is derived using superposition of static deflections. The forces on the connecting beam are reaction forces due to weight and motion of the lumped masses. They are given by Newton's second law. The combination of these results yields the equations of motion.

The static deflection y(x) of an ideal beam that is simply supported at one end and fixed at the other end when a vertical point static force F is applied at x_1 is given by (19):

$$y(x) = -\frac{1}{6\,EI}\left[W(x^3 - 3L^2x) + 3F(L - x_1)^2x\right] \qquad 0 \le x \le x_1$$

$$y(x) = -\frac{1}{6\,EI}\left[W(x^3 - 3L^2x) + F[3(L - x_1)^2x - (x - x_1)^3]\right] \quad x_1 \le x \le L$$

where

$$W = \frac{1}{2}F\left(\frac{3(L - x_1)^2L - (L - x_1)^3}{L^3}\right)$$

Using the above relationship, the beam displacement at the location of the j-th lump when a unit force is applied at the location of the i-th lump is obtained to be:

$$y_j(i) = -\frac{L^3}{2 \cdot 6^7 \cdot EI}\left[\begin{array}{l}\left(18(6 - i)^2 - (6 - i)^3\right)\left(j^3 - 3 \cdot 6^2 \cdot j\right) \\ + 6^4(6 - i)^2 \cdot j\end{array}\right], \quad j \le i$$

$$y_j(i) = -\frac{L^3}{2 \cdot 6^7 \cdot EI}\left[\begin{array}{l}\left(18(6 - i)^2 - (6 - i)^3\right)\left(j^3 - 3 \cdot 6^2 \cdot j\right) \\ + 6^4(6 - i)^2 \cdot j - 2 \cdot 6^3(j - i)^3\end{array}\right], \quad j \ge i$$

For example, the deflection of the beam at the location of the fourth lump when a unit force is applied a the location of the second lump is:

$$y_4(2) = \frac{L^3}{2 \cdot 6^7 \cdot EI} \cdot 2944$$

Using superposition, the deflection of the beam at the location of the j-th lump when forces are applied at the lump locations is:

$$y_j = \sum_{i=1}^{5} y_j(i) \cdot F_i$$

or in matrix form

$$\underline{y} = \Gamma \underline{F} \ , \tag{2.1}$$

where

$$\underline{y} = [y_1 \ y_2 \ y_3 \ y_4 \ y_5]^T$$

$$\underline{F} = [F_1 \ F_2 \ F_3 \ F_4 \ F_5]^T$$

are the deflections and the forces at the lumped masses. The flexibility matrix Γ is found to be

$$\Gamma = \frac{L^3}{2 \cdot 6^7 \cdot EI} \begin{bmatrix} 2375 & 3232 & 2781 & 1664 & 523 \\ 3232 & 5120 & 4752 & 2944 & 944 \\ 2781 & 4752 & 5103 & 3456 & 1161 \\ 1664 & 2944 & 3456 & 2816 & 1072 \\ 523 & 944 & 1161 & 1072 & 575 \end{bmatrix}$$

By applying Newton's second law to the lumped masses one obtains

$$F_i = m_L g - m_L \ddot{y}_i \quad , \quad i = 1, \ldots, 5. \tag{2.2}$$

Substituting (2.2) into (2.1) yields the equations of motion

$$\mathbf{M}\ddot{\underline{y}} + \mathbf{K}\underline{y} = \underline{F}_S \ , \tag{2.3}$$

where

$$\mathbf{M} = m_L \begin{bmatrix} 1 & 0 & 0 & 0 & 0 \\ 0 & 1 & 0 & 0 & 0 \\ 0 & 0 & 1 & 0 & 0 \\ 0 & 0 & 0 & 1 & 0 \\ 0 & 0 & 0 & 0 & 1 \end{bmatrix} = m_L \mathbf{I}$$

$$\mathbf{K} = \Gamma^{-1}$$

$$\underline{F}_S = m_L g \begin{bmatrix} 1 & 1 & 1 & 1 & 1 \end{bmatrix}^T$$

are the mass-matrix, the stiffness-matrix, and the vector of gravitational forces, respectively.

The above equation can be modified to take into account the effect of an additional disturbance at the simply supported end and the forces due to the stay cables.

The external disturbance a_Q considered here is a vertical random acceleration like that of an earthquake. It is applied at the left end of the beam (see Figures 2.1 and 2.2) and is included in the equations of motion using the following influence function (19):

$$\gamma(x) = \frac{1}{2L^3}\left[x^3 - 3L^2 x + 2L^3\right] ,$$

which is the static deflection curve of a cantilever beam for a unit displacement of the free end.

This adds the following term to the right side of the equations of motion:

$$\underline{F}_Q = -\frac{m_L}{2 \cdot 6^3}\left[\, 325 \;\; 224 \;\; 135 \;\; 64 \;\; 17 \,\right]^T a_Q \qquad (2.4)$$

The forces due to the stay cables are (2):

$$F_{C2}(t) = \frac{E_2 A_2}{L_2} \left[y_2(t) \sin \Theta_2 - u_2(t) \right] \sin \Theta_2$$

$$F_{C4}(t) = \frac{E_4 A_4}{L_4} \left[y_4(t) \sin \Theta_4 - u_4(t) \right] \sin \Theta_4 \quad , \tag{2.5}$$

where E_i, A_i, and L_i (i=2,4) are, respectively, the moduli of elasticity, the cross-sectional areas, and the lengths of the stay cables. $u_2(t)$ and $u_4(t)$ are the actuator displacements (i.e., the change in length of the cables). Θ_i (i=2,4) are the angles between the stay cables and the beam[2] . The cable forces consist of one term due to the cable stiffness and another term due to the control activity.

Define

$$\Delta K_i = \frac{E_i A_i}{l_i} \sin^2 \Theta_i \quad , \quad i = 2, 4$$

and

$$I_i = \frac{E_i A_i}{l_i} \sin \Theta_i \quad , \quad i = 2, 4$$

When the external disturbance (2.4) and the cable characteristics (2.5) are included in the original equations of motion (2.3), one gets

$$\mathbf{M}\ddot{\underline{y}} + \mathbf{K}^*\underline{y} = \underline{F}_S + \underline{F}_C + \underline{F}_Q \quad , \tag{2.6}$$

where

---

[2] The indices have been chosen to match the number of the lumped masses, where the cables are attached to.

$$K^*_{22} = K_{22} + \Delta K_2$$

$$K^*_{44} = K_{44} + \Delta K_4$$

$$\underline{F}_C = \begin{bmatrix} 0 & I_2 u_2(t) & 0 & I_4 u_4(t) & 0 \end{bmatrix}^T$$

The displacement $\underline{y}$ can be represented as the sum of the equilibrium displacement, $\underline{y}_0$, and the deviation from equilibrium, $\underline{z}$:

$$\underline{y} = \underline{y}_0 + \underline{z}$$

Without external disturbance and control and by setting the time derivatives to zero, the equations of motion (2.6) reduce to:

$$K^* \underline{y}_0 = \underline{F}_s \qquad (2.65)$$

Subtracting (2.65) from (2.6) yields the governing equation for $\underline{z}$:

$$\mathbf{M}\ddot{\underline{z}} + \mathbf{K}^* \underline{z} = \underline{F}_C + \underline{F}_Q \ , \qquad (2.7)$$

2.3 Modal Decomposition

The natural frequencies and mode shapes of the system are obtained by assuming normal mode motion

$$\underline{z}(t) = \underline{Z} \cos(\omega t + \Psi) \qquad (2.8)$$

for the homogeneous equations of motion

$$\mathbf{M}\ddot{\underline{z}} + \mathbf{K}^*\underline{z} = \underline{0} \tag{2.9}$$

Substitution of (2.8) into (2.9) yields:

$$\left[-\omega^2\mathbf{M} + \mathbf{K}^*\right]\underline{Z}\cos(\omega t + \Psi) = \underline{0}$$

For this relationship to be valid for all times t the standard eigenvalue relationship

$$\mathbf{M}^{-1}\mathbf{K}^*\underline{Z} = \lambda\underline{Z} \quad , \quad \lambda = \omega^2 \tag{2.10}$$

has to hold. The solution is the five eigenvalues λ_i and the corresponding eigenvectors $\underline{Z}_i$. The natural frequencies are:

$$\omega_i = +\sqrt{\lambda_i} \quad , \quad i = 1,\ldots,5$$

The equations of motion (2.7) can be decoupled using the modal-transformation matrix $\mathbf{\Phi}$ that contains the eigenvectors of the system as columns:

$$\mathbf{\Phi} = \left[\underline{Z}_1\ \underline{Z}_2\ \underline{Z}_3\ \underline{Z}_4\ \underline{Z}_5\right]$$

The coordinate transformation

$$\underline{z} = \mathbf{\Phi}\underline{z}^* \tag{2.11}$$

and premultiplication by $\mathbf{\Phi}^T$ result in the decoupled equations of motion

$$\mathbf{\Lambda}_M\ddot{\underline{z}}^* + \mathbf{\Lambda}_K\underline{z}^* = \underline{F}_C^* + \underline{F}_Q^* \ , \tag{2.12}$$

where

$$\Lambda_M = \Phi^T M \Phi = m_L \begin{bmatrix} 1 & 0 & 0 & 0 & 0 \\ 0 & 1 & 0 & 0 & 0 \\ 0 & 0 & 1 & 0 & 0 \\ 0 & 0 & 0 & 1 & 0 \\ 0 & 0 & 0 & 0 & 1 \end{bmatrix} = m_L I$$

$$\Lambda_K = \Phi^T K^* \Phi = \begin{bmatrix} k_1 & 0 & 0 & 0 & 0 \\ 0 & k_2 & 0 & 0 & 0 \\ 0 & 0 & k_3 & 0 & 0 \\ 0 & 0 & 0 & k_4 & 0 \\ 0 & 0 & 0 & 0 & k_5 \end{bmatrix}$$

$$\underline{F}_C^* = \Phi^T \underline{F}_C$$

$$\underline{F}_Q^* = \Phi^T \underline{F}_Q$$

The motion of the lumped masses $\underline{z}(t)$ can now be described in terms of the modal coordinates $\underline{z}^*(t)$ (2.11) which are the solutions to a set of five ordinary second order linear differential equations for the given control forces and external disturbance (2.12). The modal coordinates represent the contributions of the five modes of the system to the dynamic response:

$$\underline{z} = \underline{Z}_1 \cdot z_1^* + \underline{Z}_2 \cdot z_2^* + \underline{Z}_3 \cdot z_3^* + \underline{Z}_4 \cdot z_4^* + \underline{Z}_5 \cdot z_5^*$$

2.4 Comparison of Beam Models

To get an idea of how well the lumped-mass model (without the effect of the stay cables) describes the motion of a beam, it makes sense to compare its natural frequencies and mode shapes to those obtained using an Euler-Bernoulli beam.

The free transverse vibration of an undamped Euler-Bernoulli beam that is simply supported at one end and fixed at the other end is described by the partial differential equation (20):

$$EI\frac{\partial^4 y}{\partial x^4} + m\frac{\partial^2 y}{\partial t^2} = 0$$

subject to the boundary conditions

$$y(0, t) = 0 \quad , \quad y''(0, t) = 0$$
$$y(L, t) = 0 \quad , \quad y'(L, t) = 0$$

As before, the displacement can be represented by the sum of the equilibrium displacement, $y_0(x)$, and the deviation from equilibrium, $z(x,t)$:

$$y(x,t) = y_0(x) + z(x,t)$$

The natural frequencies ω_i, $i=1,2,\ldots$, are found from the solutions of the following frequency equation (the derivation of that equation, the natural frequencies, and the mode shapes is given in the Appendix):

$$\sin \eta L - \cos \eta L \cdot \tanh \eta L = 0 \qquad (2.13)$$

Numerical evaluation of (2.13) yields the following first five solutions:

$$\eta_1 L = 3.9266$$
$$\eta_2 L = 7.0686$$
$$\eta_3 L = 10.2102$$
$$\eta_4 L = 13.3518$$

$$\eta_5 L = 16.4934$$

Approximate solutions to (2.13) are

$$\eta_i L \approx 0.78544 + i \cdot \pi \ , \ i=1,2,3...$$

The natural frequencies are then defined by

$$\omega_i = (\eta_i L)^2 \cdot \sqrt{\frac{EI}{mL^4}} \ , \ i = 1,2,... \qquad (2.14)$$

The mode shapes are given by

$$\beta_i(x) = H_i\left[\sin \eta_i x - \frac{\sin \eta_i L}{\sinh \eta_i L} \sinh \eta_i x\right] \ , \ i = 1,2,... \qquad (2.15)$$

where the H_i's are arbitrary constants.

In order to get a comparable expression for the natural frequencies of the lumped-mass model, the standard eigenvalue relationship (2.10) is solved in the following, modified[3] form:

$$2 \cdot 6^8 \cdot \begin{bmatrix} 2375 & 3232 & 2781 & 1664 & 523 \\ 3232 & 5120 & 4752 & 2944 & 944 \\ 2781 & 4752 & 5103 & 3456 & 1161 \\ 1664 & 2944 & 3456 & 2816 & 1072 \\ 523 & 944 & 1161 & 1072 & 575 \end{bmatrix}^{-1} \underline{Z} = \mu \underline{Z} \ ,$$

where

[3] The original stiffness matrix (2.3) without the effect of the bridge cables is used and the parameters E, I, m, and L remain explicitly in μ.

$$\mu = \frac{mL^4}{EI}\omega^2 \tag{2.16}$$

One obtains the eigenvalues

$$\mu_1 = 0.02376 \cdot 10^4$$

$$\mu_2 = 0.24851 \cdot 10^4$$

$$\mu_3 = 1.05725 \cdot 10^4$$

$$\mu_4 = 2.83373 \cdot 10^4$$

$$\mu_5 = 5.13801 \cdot 10^4$$

and the mode shapes (rounded to the 2nd digit)

$$\underline{Z}_1 = \begin{bmatrix} -0.36 \\ -0.59 \\ -0.59 \\ -0.40 \\ -0.14 \end{bmatrix}, \quad \underline{Z}_2 = \begin{bmatrix} 0.53 \\ 0.40 \\ -0.23 \\ -0.62 \\ -0.35 \end{bmatrix}, \quad \underline{Z}_3 = \begin{bmatrix} -0.57 \\ 0.15 \\ 0.53 \\ -0.30 \\ -0.53 \end{bmatrix}, \quad \underline{Z}_4 = \begin{bmatrix} 0.45 \\ -0.54 \\ 0.20 \\ 0.30 \\ -0.61 \end{bmatrix}, \quad \underline{Z}_5 = \begin{bmatrix} 0.23 \\ -0.42 \\ 0.53 \\ -0.53 \\ 0.46 \end{bmatrix}$$

Using (2.14) and (2.16) the natural frequencies of the Euler-Bernoulli beam model and the lumped-mass model can be compared directly (Table 2.1). It is seen that the natural frequencies of the lumped-mass model are all lower than those of the Euler-Bernoulli beam model. The relative error increases toward higher modes with a maximum error for the fifth natural frequency of approximately -20 percent. There the approximation of the beam by the lumped masses reaches its limitations. The relatively high error in the fifth mode can be tolerated, since the system response is dominated by the lower modes. This will be demonstrated in the next section of this chapter.

i	Euler-Bernoulli beam $\frac{\omega_i}{\sqrt{\frac{EI}{mL^4}}}$	Lumped-mass model $\frac{\omega_i}{\sqrt{\frac{EI}{mL^4}}}$	Error in %
1	15.4182	15.4157	-0.01
2	49.9649	49.8512	-0.22
3	104.2477	102.8229	-1.38
4	178.2697	168.3368	-5.90
5	272.0310	226.6717	-20.01

Table 2.1: Comparison of Natural Frequencies

A comparison of the mode shapes is shown in Figure 2.3. The mode shapes of the Euler-Bernoulli beam (2.15) are plotted with H_i=1 and the values of the mode shape vectors of the lumped-mass model are plotted at the respective location of the lumped masses[4] . The result is quite good, as the values of the mode shape vectors are almost identical to the values of the mode shapes of the Euler-Bernoulli beam at the location of the lumped masses.

[4] The mode shape vectors were rescaled for comparison.

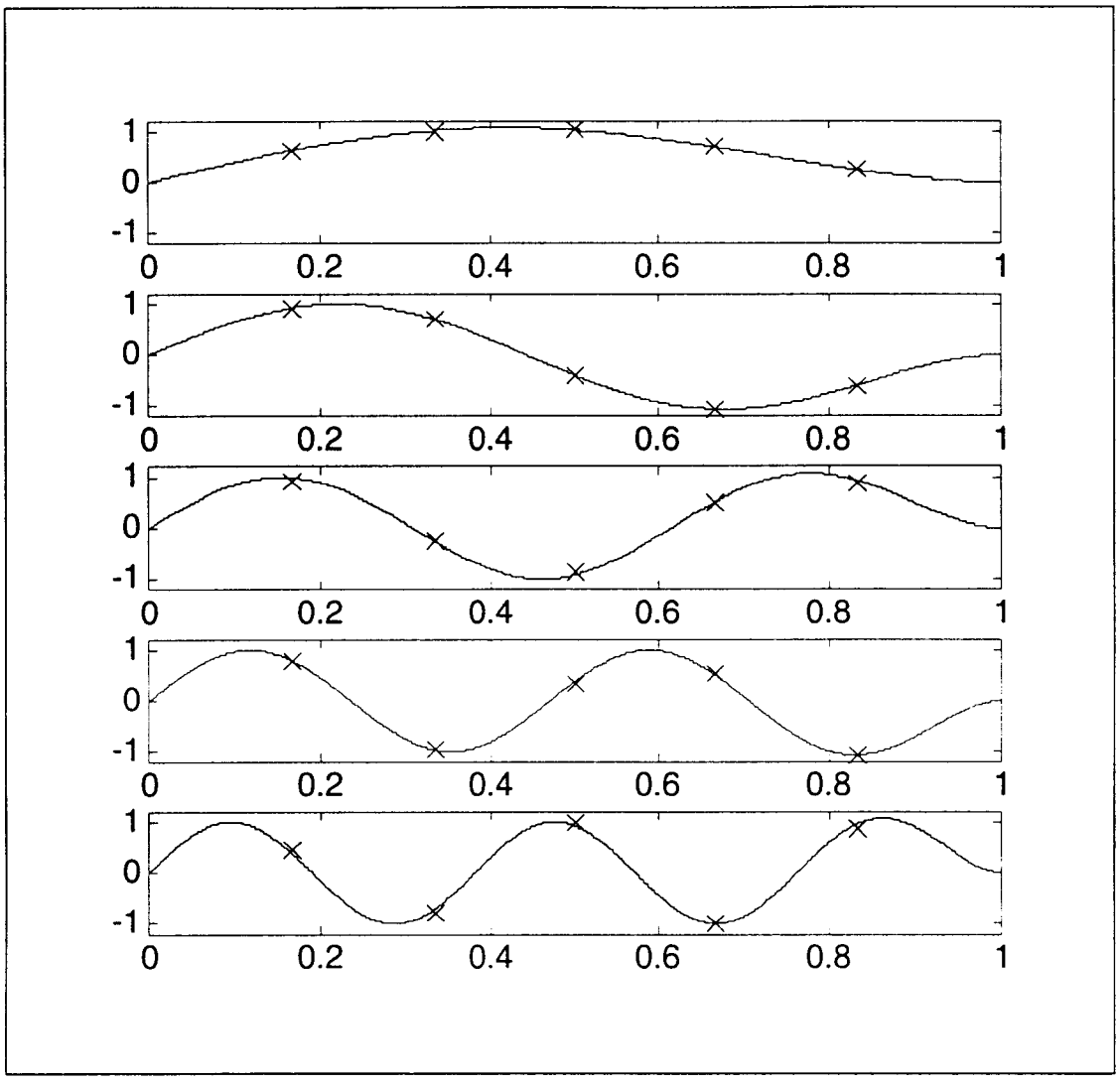

Figure 2.3: Comparison of mode shapes

In conclusion, the natural frequencies and mode shapes of the introduced lumped-mass model compare very well to the first five natural frequencies and mode shapes of the Euler-Bernoulli beam model. Therefore the lumped-mass model can be used to simulate the response of the beam, due to an external disturbance.

2.5 Response of the Uncontrolled Beam to an External Disturbance

Here the responses of both the lumped-mass model and the Euler-Bernoulli beam model to an external disturbance are obtained to, once again, demonstrate the close correspondence of the two models and as a comparison for the response of the controlled structure later on.

The following parameters were used:

modulus of elasticity of beam (steel)	E	$= 2.07 \cdot 10^{11}$ N/m^2
moment of inertia	I	$= 0.54$ m^4
mass per unit length	m	$= 3.642 \cdot 10^3$ kg/m
length of beam	L	$= 70$ m
modulus of elasticity of cables	$E_{2,4}$	$= 1.655 \cdot 10^{11}$ N/m^2
cross-section of cables	$A_{2,4}$	$= 3.526 \cdot 10^{-3}$ m^2
length of left cable	L_2	$= 84.13$ m
length of right cable	L_4	$= 73.79$ m
angle between deck and left cable	Θ_2	$= 0.9828$ rad
angle between deck and right cable	Θ_4	$= 1.2490$ rad

These parameters approximately represent a left-end girder of a typical cable-stayed bridge (21).

Consequently,

$$m_L = 42{,}490.00 \text{ kg}$$

$$\mathbf{K}^* = \begin{bmatrix} 0.6953 & -0.6693 & 0.2926 & -0.0788 & 0.0225 \\ -0.6693 & 0.9940 & -0.7481 & 0.3151 & -0.0900 \\ 0.2926 & -0.7481 & 1.0104 & -0.7594 & 0.3376 \\ -0.0788 & 0.3151 & -0.7594 & 1.0420 & -0.8381 \\ 0.0225 & -0.0900 & 0.3376 & -0.8381 & 1.3255 \end{bmatrix} \cdot 10^9 \frac{\text{N}}{\text{m}}$$

$$I_2 = 5.7714 \cdot 10^6 \frac{N}{m}$$

$$I_4 = 7.5027 \cdot 10^6 \frac{N}{m}$$

$$\underline{F_0} = -\begin{bmatrix} 3.1966 \\ 2.2032 \\ 1.3278 \\ 0.6295 \\ 0.1672 \end{bmatrix} \cdot 10^4\, kg \cdot a_0$$

The external disturbance used here is the El Centro earthquake record (El Centro, May 18, 1940, S00E: amax=3.4 m/s^2) scaled by a factor of five in order to dramatize the effect. The accelerogram is shown in Figure 2.4.

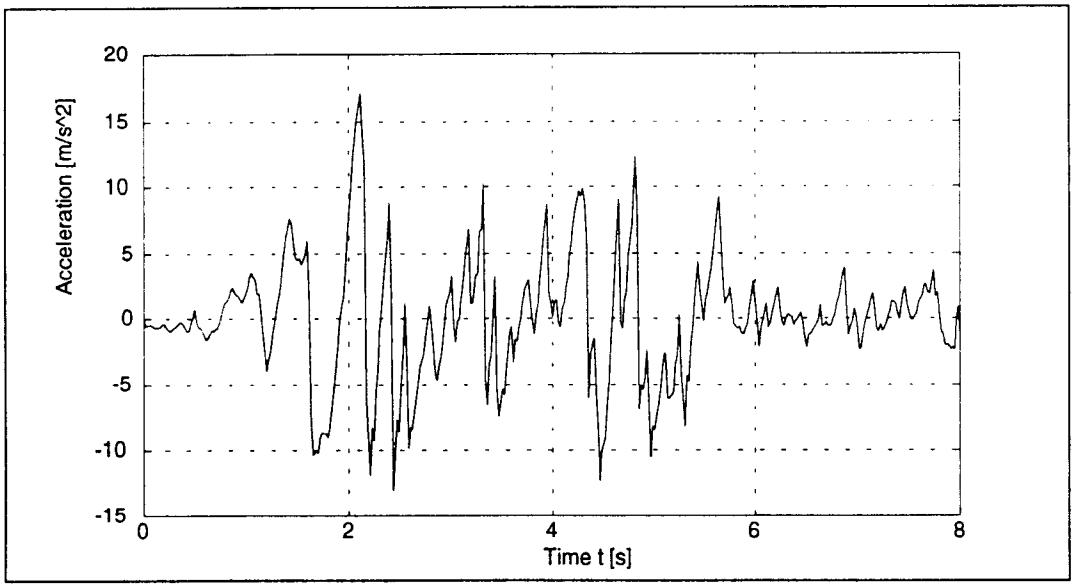

Figure 2.4: Earthquake accelerogram

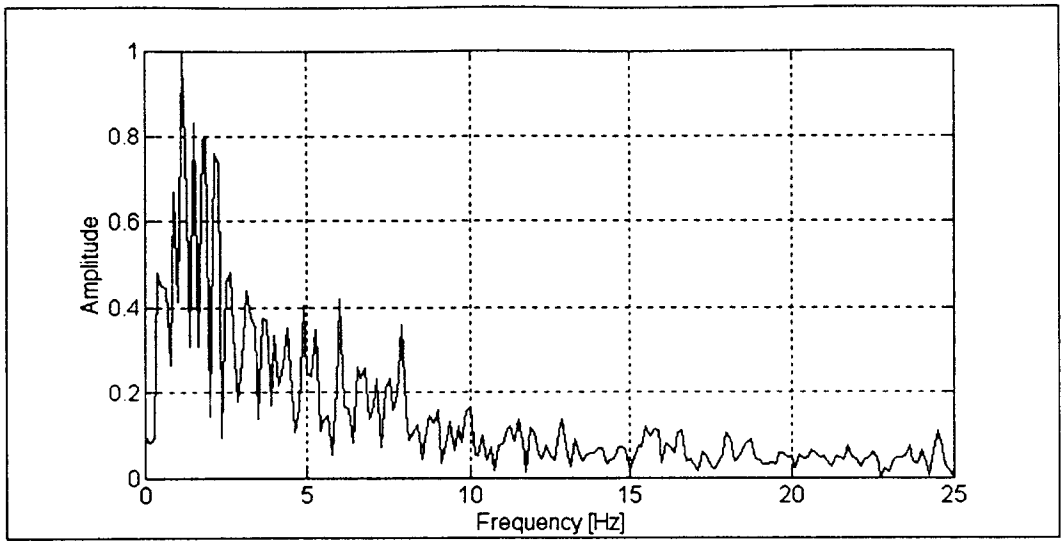

Figure 2.5: Periodogram of earthquake acceleration

The periodogram of the earthquake acceleration is shown in Figure 2.5. Clearly, most of the earthquake's energy is concentrated around the low end of the frequency spectrum. Since the first natural frequency of the beam structure is approximately 6 Hz one can conclude that the dynamic response of the structure to an external disturbance of this kind will be dominated by the lower modes.

The simulations are performed using MATLAB™. The sampling frequency of the earthquake data is 50 Hz. The acceleration is assumed to be constant between samples. For the Euler-Bernoulli beam, the beam motion is approximated by using the first ten modes and then integrating the resulting set of coupled second order linear differential equations using a 4th and 5th order Runge-Kutta algorithm with a tolerance of 1e-6. The solution of the lumped-mass model is obtained by integrating the equations of motion (2.7) using the same algorithm.

The results of the simulations are shown in Figure 2.6. As it was expected, the results are in good agreement.

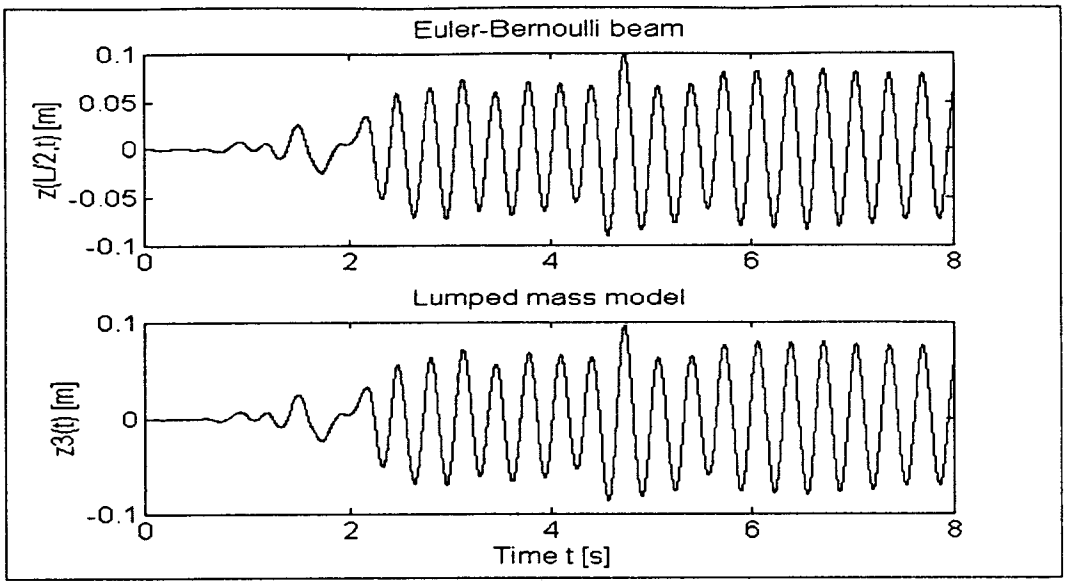

Figure 2.6: Uncontrolled midspan displacement

Figure 2.7 shows the periodogram of the midspan displacement of the uncontrolled beam structure. As it was expected the lower modes dominate the system response.

In the following chapter control of the system in a decentralized fashion is investigated.

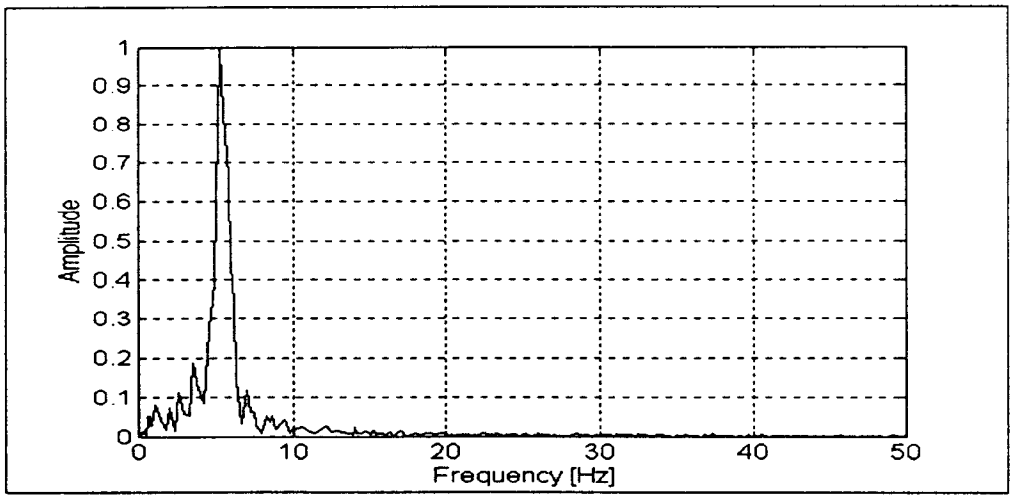

Figure 2.7: Periodogram of uncontrolled midspan displacement

3. The Control Strategy

In this chapter a decentralized control strategy is proposed to enhance the stability of the beam structure. Stability of the controlled system is shown by calculation of the closed loop eigenvalues. An outline of a theoretical proof of stability is also given. The performance of the control is demonstrated through computer simulations.

3.1 Decentralized Control

Decentralized control emerged from the trend to control systems of increasing complexity. The fundamental characteristics of complex systems are dimensionality, uncertainty, and information structure constraints (16). In general a decentralized control approach has the following characteristics:

1) A complex system is decomposed into a number of interconnected subsystems. This decomposition may be a natural result of the physical properties of the system itself. In this case, the subsystems are simply the components that make up the overall system. On the other hand, the decomposition can be mathematical in nature, where the resulting subsystems have no physical meaning.

2) Instead of using a centralized control approach, where global system information is used to compute the control signals for all the actuators, the subsystems are controlled independently. The resulting controllers use local information to compute the control signals that drive local actuators. Therefore, decentralized control results in

lower-dimensional controllers that are easier to implement, and can be used to address information structure constraints or reduce the amount of information that needs to be transmitted.

A common approach is to stabilize each subsystem independently and then show that this stabilizes the overall system.

3.2 Decomposition of the Model

The lumped masses of the model introduced in the previous chapter can be interpreted as five interconnected subsystems. The control forces are applied to two of those subsystems through the actuators that are attached to the ends of the cables at the anchor points.

Define the state variables

$$\underline{s}_i = \left[z_i \ \dot{z}_i\right]^T, \quad i=1,2,3,4,5 \tag{3.1}$$

Using the equations of motion (2.7) the state-equations for each subsystem can be expressed as follows:

$$\dot{\underline{s}}_i = \mathbf{A}_i \underline{s}_i + \sum_{\substack{j=1 \\ j\neq i}}^{5} \mathbf{A}_{ij} \underline{s}_j + \underline{E}_i a_Q \ , \quad i=1,3,5$$

$$\dot{\underline{s}}_i = \mathbf{A}_i \underline{s}_i + \underline{b}_i u_i + \sum_{\substack{j=1 \\ j\neq i}}^{5} \mathbf{A}_{ij} \underline{s}_j + \underline{E}_i a_Q \ , \quad i=2,4 \ , \tag{3.2}$$

where

$$\mathbf{A}_i = \begin{bmatrix} 0 & 1 \\ -\frac{K_{ii}^*}{m_L} & 0 \end{bmatrix}, \quad i=1,2,3,4,5$$

$$\underline{b}_i = \begin{bmatrix} 0 \\ \frac{I_i}{m_L} \end{bmatrix}, \quad i=2,4$$

$$\mathbf{A}_{ij} = \begin{bmatrix} 0 & 0 \\ -\frac{K_{ij}^*}{m_L} & 0 \end{bmatrix}, \quad i,j=1,2,3,4,5 \ , \ i \neq j$$

$$\underline{E}_i = \begin{bmatrix} 0 \\ \frac{e_i}{m_L} \end{bmatrix}, \quad i=1,2,3,4,5$$

The $\mathbf{A}_i$, $\underline{b}_i$, $\mathbf{A}_{ij}$, and $\underline{E}_i$ are the system matrices of the individual subsystems, the control input vectors, the interconnection matrices, and the influence vectors of the external disturbance respectively. The e_i's are obtained from (2.4).

3.3 The Control Law

The beam has been modeled without internal damping. However, in every physical system of this kind, there is always a certain degree of internal damping present. Therefore one should keep in mind that, although the open-loop poles of the subsystems and the overall system model are located on the imaginary axis, in a real system the open-loop poles would be located in the open left half of the complex plane, i.e., the system would be asymptotically stable.

An intuitive approach to increase the system's stability against external disturbances is to introduce active damping into the system by means of decentralized velocity-feedback control, where forces are applied in the opposite direction of the bridge motion. The controllers for the subsystems 2 and 4 are then given by:

$$u_i(t) = -\begin{bmatrix} 0 & f_i \end{bmatrix} \underline{s}_i \quad , \quad f_i>0, \quad i=2,4 \qquad (3.3)$$

The closed-loop equations of the overall system are obtained by substituting (3.3) into (2.7) with the use of the state variable definition (2.1):

$$\mathbf{M}\ddot{\underline{z}} + \mathbf{C}\dot{\underline{z}} + \mathbf{K}^*\underline{z} = \underline{F}_Q \quad ,$$

where

$$\mathbf{C} = \begin{bmatrix} 0 & 0 & 0 & 0 & 0 \\ 0 & c_2 & 0 & 0 & 0 \\ 0 & 0 & 0 & 0 & 0 \\ 0 & 0 & 0 & c_4 & 0 \\ 0 & 0 & 0 & 0 & 0 \end{bmatrix}$$

and

$$c_i = \frac{I_i \cdot f_i}{m_L} \quad , \quad i=2,4 \quad .$$

The introduction of damping directly affects only the subsystems 2 and 4. The uncontrolled subsystems are affected indirectly through the interconnections. Stability of the overall system depends on the characteristics of the interconnections. The restoring forces of the model are always directed toward the equilibrium positions of the lumped masses. Therefore initially a stabilizing effect of

the proposed control is expected. For large values of the c_i's, i.e., for large control forces, instability may occur due to inertial effects.

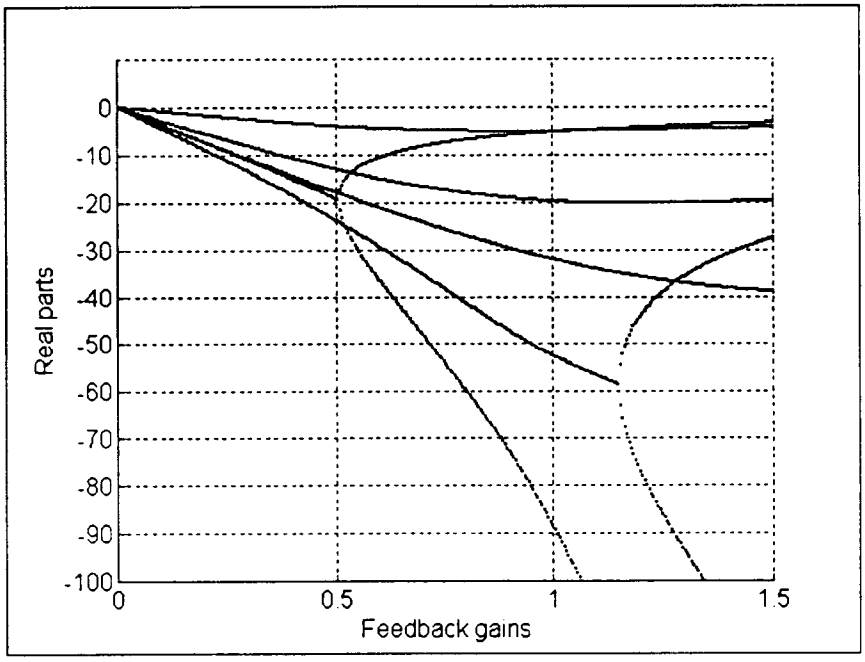

Figure 3.1: Generalized root locus

Figure 3.1 shows a generalized root locus plot of the controlled system. There the velocity feedback gain[1] is plotted versus the real parts of the closed-loop eigenvalues. It is seen that at first damping increases in all the modes for increasing feedback gain. The fact that damping increases with different rates for each mode can be explained in terms of the system parameters and the actuator locations. First, the different cable lengths and angles for subsystem 2 and 4 result in different influence constants (I_2 and I_4). Also the control forces have different effects on the system modes in correspondence with the mode shapes.

[1] The same velocity feedback gain was used for both controllers.

The study of the generalized root locus shows, that the decentralized velocity feedback control is capable of introducing active damping into the system, thus making it asymptotically stable. It also suggests that there exist certain optimal feedback gains with respect to control activity versus reduction of vibrations. These optimal gains should be affected by the system parameters, the actuator locations, and also the influence vector of the external disturbance.

3.4 Proof of Stability (Outline)

The calculation of the closed-loop eigenvalues as shown in Figure 3.1 proves that the proposed decentralized control indeed stabilizes the system.

A theoretical proof of the system stability is a problem which has been addressed by many researchers (16, 22-24). Here the theory developed by Šiljak (16), who established the concept of 'connective stability' of a system that consists of interconnected subsystems is used. Although the proof is not performed here it can be used as an argument for the success of the proposed control strategy.

The proof uses the Matrosov-Bellman concept of vector Liapunov functions where a Liapunov function for each individual subsystem is used as a component of a vector function. This vector function then establishes stability of the overall system. The result of the proof is a test matrix **W**. The system is connectively stable if this matrix belongs to the class of M-matrices (16) that possesses certain properties.

In the so-called linear construction of a vector Liapunov function for a linear system that has the interconnection

characteristics of the beam model considered here (3.2) a norm-like function defined as

$$v_i(\underline{s}_i) = \left(\underline{s}_i^T \mathbf{H}_i \underline{s}_i\right)^{1/2}$$

is used, where $\mathbf{H}_i$ is a constant, symmetric, and positive definite solution to the Liapunov equation associated with the i-th subsystem, that is

$$\mathbf{A}_i^T \mathbf{H}_i + \mathbf{H}_i \mathbf{A}_i = -\mathbf{S}_i \ ,$$

for a given $\mathbf{S}_i$ which is also a constant, symmetric, and positive definite matrix.

The elements of the test matrix $\mathbf{W}$ are obtained to be

$$w_{ij} = \begin{cases} \dfrac{1}{2}\dfrac{\lambda_m(\mathbf{S}_i)}{\lambda_M(\mathbf{H}_i)}, & i = j \\ -\lambda_M^{1/2}(\mathbf{A}_{ij}^T \mathbf{A}_{ij}), & i \neq j \end{cases} ,$$

where $\lambda_m()$ and $\lambda_M()$ are, respectively, the minimum and maximum eigenvalue of the corresponding matrix. The terms $\lambda_M^{1/2}(\mathbf{A}_{ij}^T \mathbf{A}_{ij})$ are bounds of the interconnections and the terms $\lambda_m(\mathbf{S}_i)/\lambda_M(\mathbf{H}_i)$ are estimates of the stability of the isolated subsystems. Šiljak remarks, that the larger the diagonal elements w_{ii} and the smaller the off-diagonal elements w_{ij} of $\mathbf{W}$, the better are the chances for $\mathbf{W}$ to be an M-matrix.

Since in the case of the beam system considered here all the subsystems are asymptotically stable to begin with (the beam actually possesses internal damping), it is always possible to find the matrices $\mathbf{H}_i$. One can then argue that the use of decentralized velocity feedback on subsystems 2

and 4 increases their degree of stability thus making the diagonal elements w_{22} and w_{44} of **W** larger. This in turn increases the chance of the overall system to be connectively stable.

3.5 Controller Performance

In order to assess the performance of the proposed controller a feedback gain of 0.6 is used for simulation purposes. The generalized root locus in Figure 3.1 shows that this introduces damping into all the system modes.

The simulated system response is shown in the following plots. Figure 3.2 compares the uncontrolled and controlled beam motion.

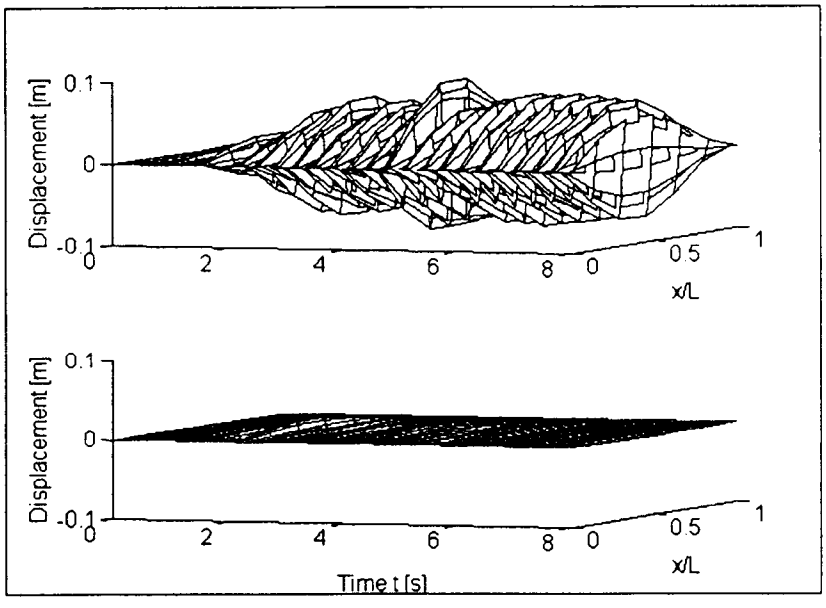

Figure 3.2: Uncontrolled and controlled beam motion

The reduction of the beam vibration is apparent. In this case the maximum amplitude of the beam motion is reduced by approximately a factor of 7.

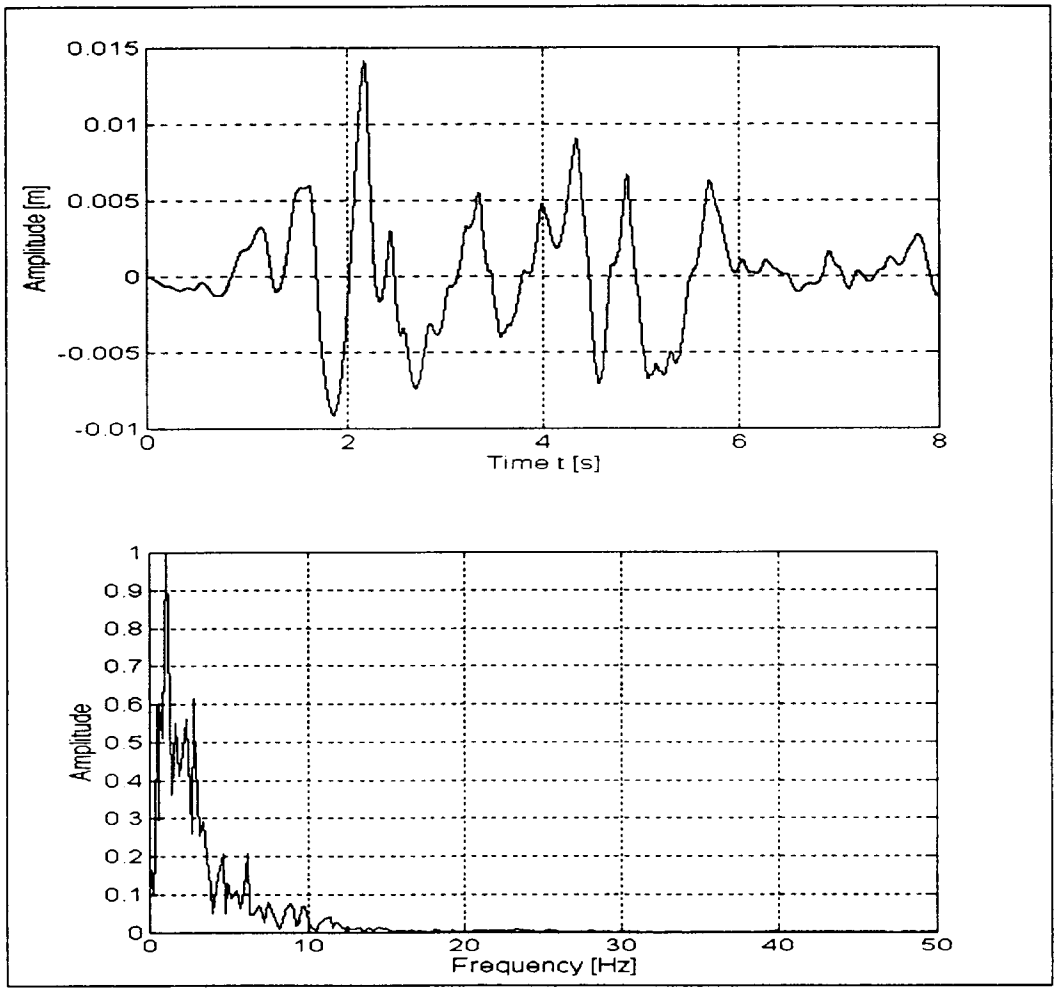

Figure 3.3: Midspan displacement/periodogram of controlled beam structure

Figure 3.3 shows the midspan displacement of the controlled beam structure together with the corresponding periodogram. The first mode vibration of the structure has been successfully reduced.

The control displacements are shown in Figure 3.4.

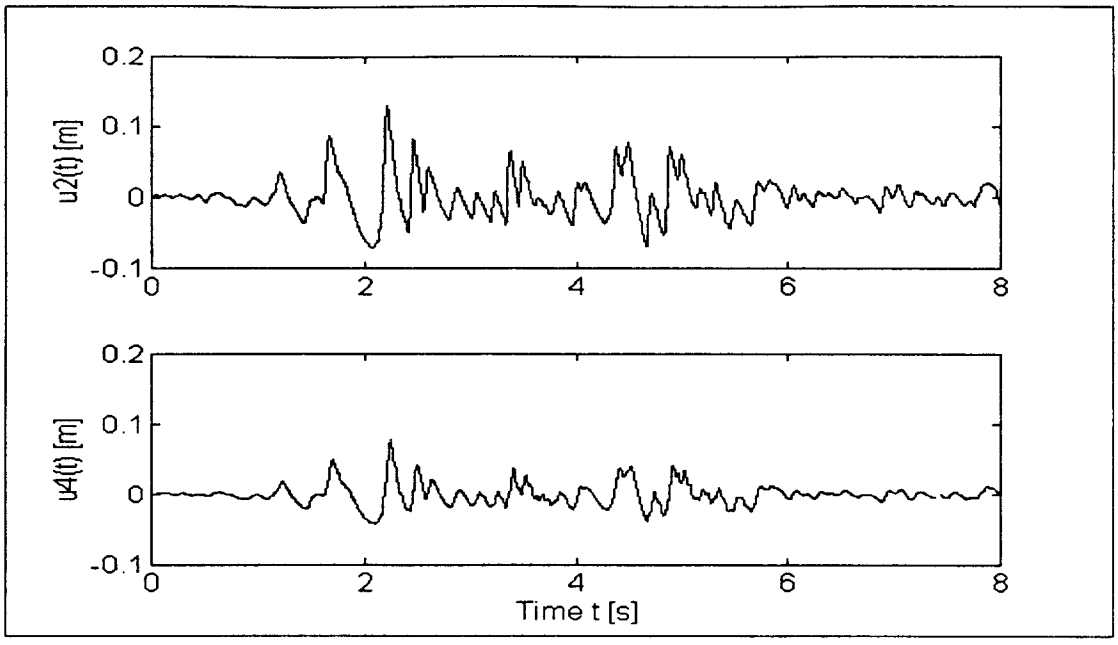

Figure 3.4: Control displacements

The following simulations are intended as an initial study of the sensitivity of the proposed control to variations in the parameters and structure of the model. There the value of m was increased by 10 percent and the values of EI, E_2A_2, and E_4A_4 were decreased by 10 percent. To reflect uncertainties in the interconnections of the system the values of the elements of the flexibility matrix Γ were randomly varied within 1 percent of their nominal value in (2.1).

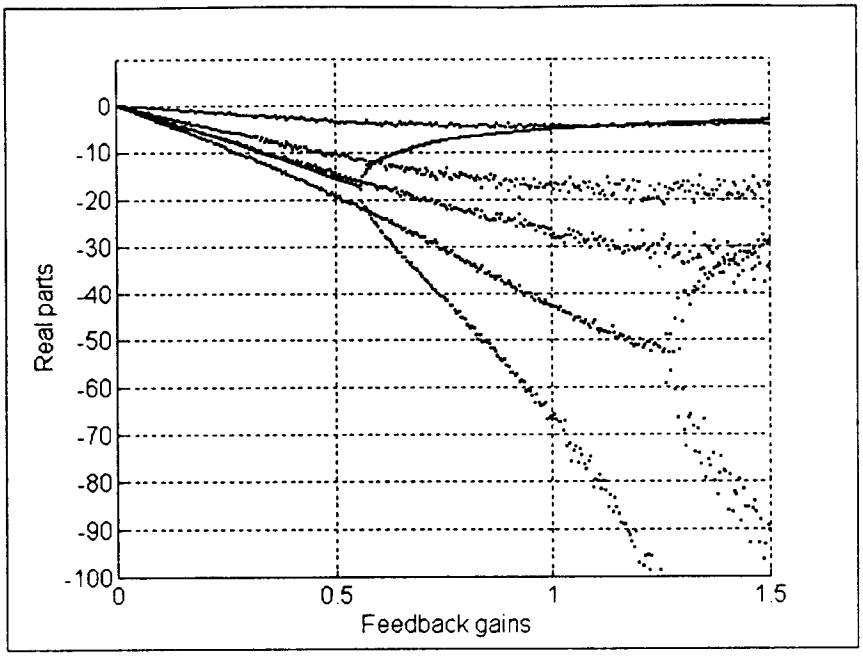

Figure 3.5: Generalized root locus of perturbed model

Figure 3.5 shows the generalized root locus of the perturbed model. The random variation of the flexibility matrix is performed for each calculation in order to visualize the regions in which the closed loop eigenvalues are located. Some deterioration compared to Figure 3.1 is visible, but the introduction of damping into all the modes is still achieved.

Again a feedback gain of 0.6 is used to simulate the response of the controlled beam. As shown in Figure 3.6 the reduction of the beam vibration is still significant.

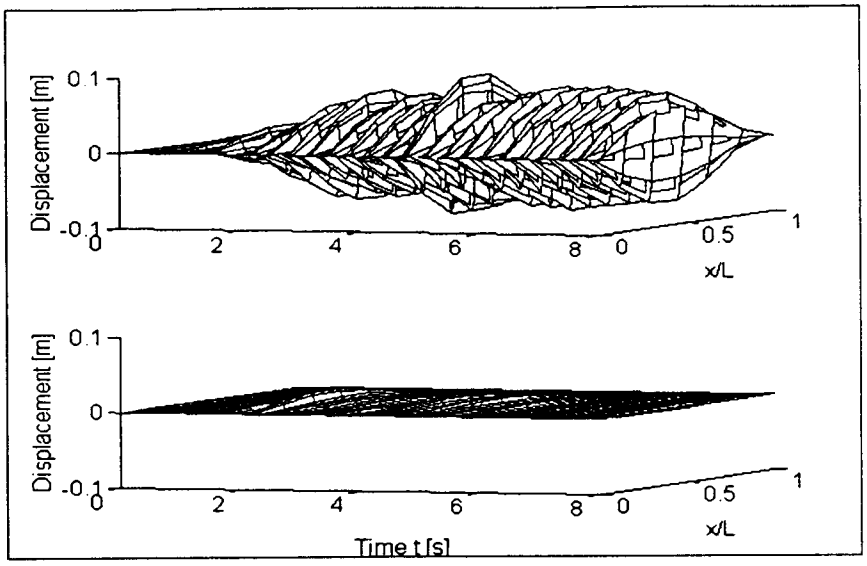

Figure 3.6: Uncontrolled and controlled beam motion of perturbed model

3.6 Optimal Control of Subsystems

In the previous section, the decentralized velocity feedback gains have been chosen based on the study of the systems closed loop eigenvalues. Here the theory of linear optimal control is applied to the two controlled subsystems. A methodology is suggested of how the structure of the system can be incorporated into the design of the two subsystem regulators by an appropriate choice of the associated weighting matrices.

3.6.1 The Regulator Problem

The theory of design of linear quadratic regulators (LQG) for linear time-invariant linear systems is well known and can be found in many textbooks on control systems (e.g.,

(25)). It is briefly stated here for the convenience of the reader.

The optimal linear feedback control $\underline{u}^*$ for the linear time-invariant system

$$\dot{\underline{s}} = \mathbf{A}\underline{s} + \mathbf{B}\underline{u}$$

that minimizes the performance index

$$V = \int_0^\infty (\underline{u}^T \mathbf{R} \underline{u} + \underline{s}^T \mathbf{Q} \underline{s}) \, dt$$

is given by

$$\underline{u}^* = - \mathbf{G} \, \underline{s} = - \mathbf{R}^{-1} \mathbf{B}^T \overline{\mathbf{P}} \, \underline{s} \ , \qquad (3.4)$$

where $\overline{\mathbf{P}}$ is the solution to the algebraic Ricatti equation

$$\overline{\mathbf{P}}\mathbf{A} + \mathbf{A}^T\overline{\mathbf{P}} - \overline{\mathbf{P}}\mathbf{B}\mathbf{R}^{-1}\mathbf{B}^T\overline{\mathbf{P}} + \mathbf{Q} = 0 \ . \qquad (3.5)$$

A and **B** are the system matrix and the input distribution matrix. $\underline{s}$ and $\underline{u}$ are the system state and the control input. The matrices **R** and **Q** are weighting matrices that penalize the control activity and the system states. **R** is a symmetric positive definite matrix and **Q** is a symmetric semi definite matrix. **G** is the optimal control gain matrix.

The solution of the Ricatti equation (3.5) exists and the closed-loop system is guaranteed to be asymptotically stable under the following assumptions:

1) The pair (**A**,**B**) is stabilizable.

2) The pair $(\mathbf{A},\mathbf{D})$ is detectable, where $\mathbf{D}$ is any matrix or vector such that $\mathbf{DD}^T = \mathbf{Q}$.

3.6.2 Subsystem Controller Design

The results of the previous section are now applied to the subsystems 2 and 4, ignoring the coupling with the other subsystems. These are controllable second order systems given by

$$\dot{\underline{s}}_i = \mathbf{A}_i \underline{s}_i + \underline{b}_i u_i = \begin{bmatrix} 0 & 1 \\ -\dfrac{K^*(i,i)}{m_L} & 0 \end{bmatrix} \underline{s}_i + \begin{bmatrix} 0 \\ \dfrac{I_i}{m_L} \end{bmatrix} u_i \quad , \quad i=2,4$$

Therefore the weighting matrices for the control $\mathbf{R}_i = r_i$ $(i=2,4)$ are scalars and the weighting matrices for the states $\mathbf{Q}_i$ $(i=2,4)$ are 2 by 2 matrices.

The selection of the weighting matrices will influence the resulting feedback control gains and the resulting closed-loop performance of the system. The $\mathbf{Q}_i$'s are initially chosen to be

$$\mathbf{Q}_i = \begin{bmatrix} 1 & 0 \\ 0 & 1 \end{bmatrix} \quad , \quad i=2,4$$

The initial choice for the r_i's is

$$r_i = 1 \quad , \quad i=2,4$$

The results for the subsystem feedback gains are (using the parameters from Chapter 2):

$$\underline{G}_2 = [0.0029 \quad 1.0000]$$

$$\underline{G}_4 = [0.0036 \quad 1.0000]$$

It is interesting to note, that the results are mostly velocity feedback. If the $\mathbf{Q}_i$'s are chosen to be

$$\mathbf{Q}_i = \begin{bmatrix} 0 & 0 \\ 0 & 1 \end{bmatrix} , \quad i=2,4 ,$$

which is a possible choice, the resulting feedback gains are:

$$\underline{G}_2 = [0 \; 1]$$

$$\underline{G}_4 = [0 \; 1]$$

The result is pure velocity feedback. Therefore the decentralized velocity feedback can be interpreted as optimal control of the subsystems minimizing some norm of the subsystem velocity and the control.

The remaining weights can be used to consider the structural differences between the two subsystems. For instance, the control input coefficients I_2 and I_4 are different, namely

$$\frac{I_4}{I_2} = 1.3 ,$$

meaning that the same feedback gain has a greater impact on subsystem 4 than on subsystem 2. By choosing

$$r_4 = \left(\frac{I_4}{I_2}\right)^2$$

the feedback gain for subsystem 4 becomes

$$\underline{G}_4 = \begin{bmatrix} 0 & \frac{I_2}{I_4} \end{bmatrix}$$

In this way the structural difference has been equalized.

The impact of the external disturbance and the form of the mode shapes could be used for further weight variations. More study is needed in this direction.

3.6.3 Global Optimal Control

In order to compare the decentralized result of the previous section to a global control strategy it is now assumed that all the system states are available for feedback and the theory of Chapter 3.5.1 is applied to the overall system

$$\dot{\underline{s}} = \mathbf{A}\underline{s} + \mathbf{B}\underline{u} \ ,$$

where

$$\underline{s} = \begin{bmatrix} \underline{z} \\ \dot{\underline{z}} \end{bmatrix}$$

$$\underline{u} = \begin{bmatrix} u_2 \\ u_4 \end{bmatrix}$$

$$\mathbf{A} = \begin{bmatrix} \mathbf{0} & \mathbf{I} \\ -\mathbf{M}^{-1}\mathbf{K} & \mathbf{0} \end{bmatrix}$$

$$\mathbf{B} = \begin{bmatrix} 0\ 0\ 0\ 0\ 0\ 0 & \left(\frac{I_2}{m_L}\right) & 0 & 0 & 0 \\ 0\ 0\ 0\ 0\ 0\ 0 & 0 & 0 & \left(\frac{I_4}{m_L}\right) & 0 \end{bmatrix}^T$$

0 and **I** are, respectively, the zero matrix and the identity matrix of appropriate dimension.

A similar performance index with

$$\mathbf{R} = \begin{bmatrix} 1 & 0 \\ 0 & \left(\frac{I_4}{I_2}\right)^2 \end{bmatrix}$$

$$\mathbf{Q} = \begin{bmatrix} 0&0&0&0&0&0&0&0&0&0 \\ 0&0&0&0&0&0&0&0&0&0 \\ 0&0&0&0&0&0&0&0&0&0 \\ 0&0&0&0&0&0&0&0&0&0 \\ 0&0&0&0&0&0&0&0&0&0 \\ 0&0&0&0&0&1&0&0&0&0 \\ 0&0&0&0&0&0&1&0&0&0 \\ 0&0&0&0&0&0&0&1&0&0 \\ 0&0&0&0&0&0&0&0&1&0 \\ 0&0&0&0&0&0&0&0&0&1 \end{bmatrix}$$

is used to solve the associated algebraic Ricatti equation to obtain the feedback gain matrix

$$\mathbf{G} = \begin{bmatrix} -58.94 & 63.18 & -34.62 & 5.26 & 17.10 & -0.08 & 1.38 & 0.13 & -0.01 & -0.03 \\ 40.16 & -7.85 & -46.49 & 58.79 & -45.43 & 0.14 & -0.01 & -0.19 & 1.12 & 0.19 \end{bmatrix}$$

which renders the closed loop system asymptotically stable.

Here position feedback clearly dominates velocity feedback. It is also noted that the maximum gains are found at the actuator locations.

3.6.4 Comparison of Decentralized and Global Control

The following figures show the midspan displacements and the control displacements of the decentrally controlled system using the feedback gains

$$\underline{G}_2 = [0\ 1]$$

$$\underline{G}_4 = \begin{bmatrix} 0 & \frac{I_2}{I_4} \end{bmatrix}$$

and the system controlled by the global feedback matrix **G** of the previous section.

The decentralized control results in comparable reduction of the midspan vibration and similar control displacements.

The actuator activity for the global control is more evenly distributed between the two actuators compared to the actuator activity of the decentralized control. This is a possible drawback of the decentralized approach but can be taken into consideration by the actuator specifications.

One also has to keep in mind that the slightly better performance of the global approach comes to a price. Sensors have to be installed at the locations of all the lumped masses and the additional information has to be transmitted to the controller.

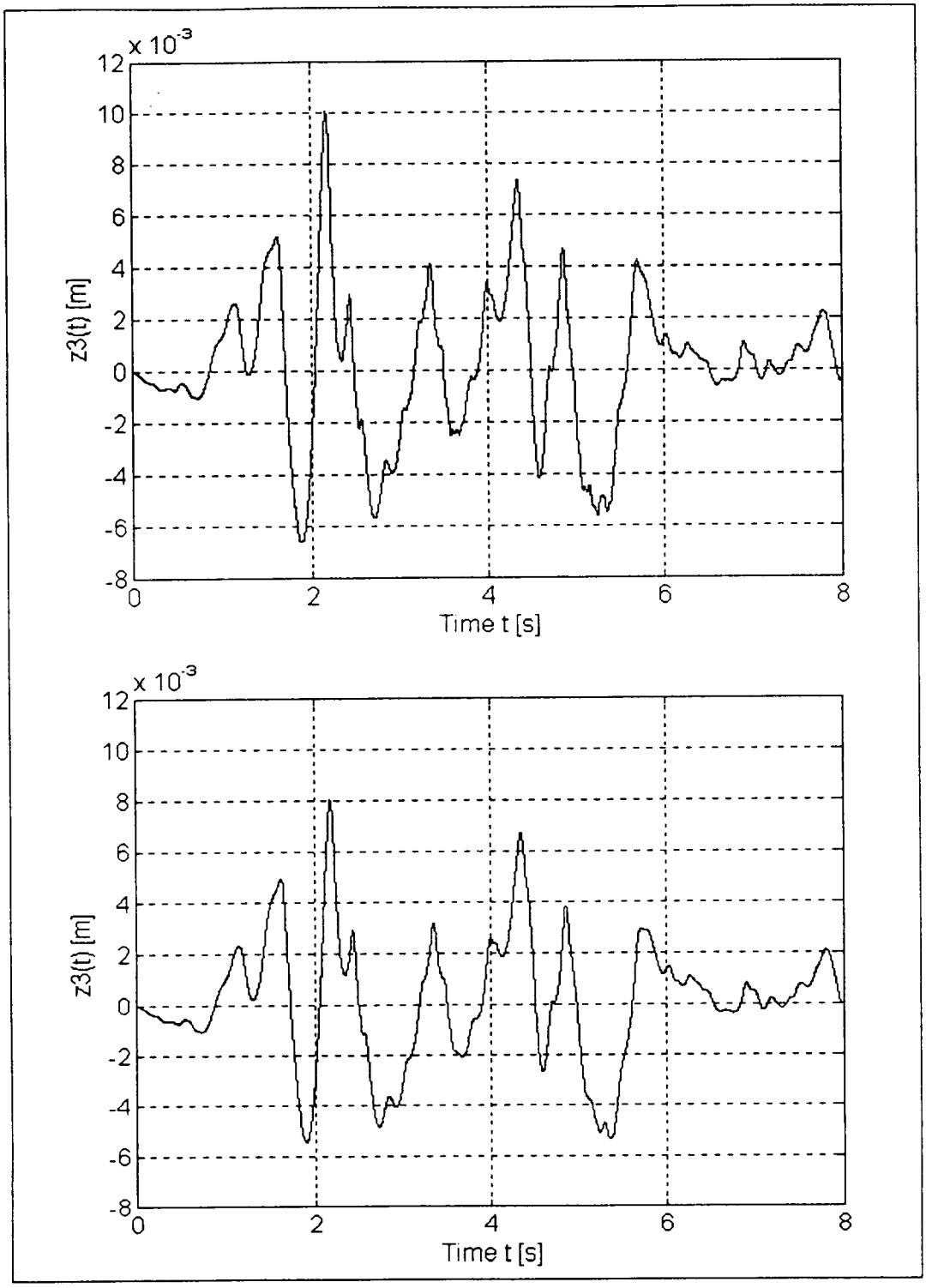

Figure 3.7: Midspan displacements of decentralized and global control

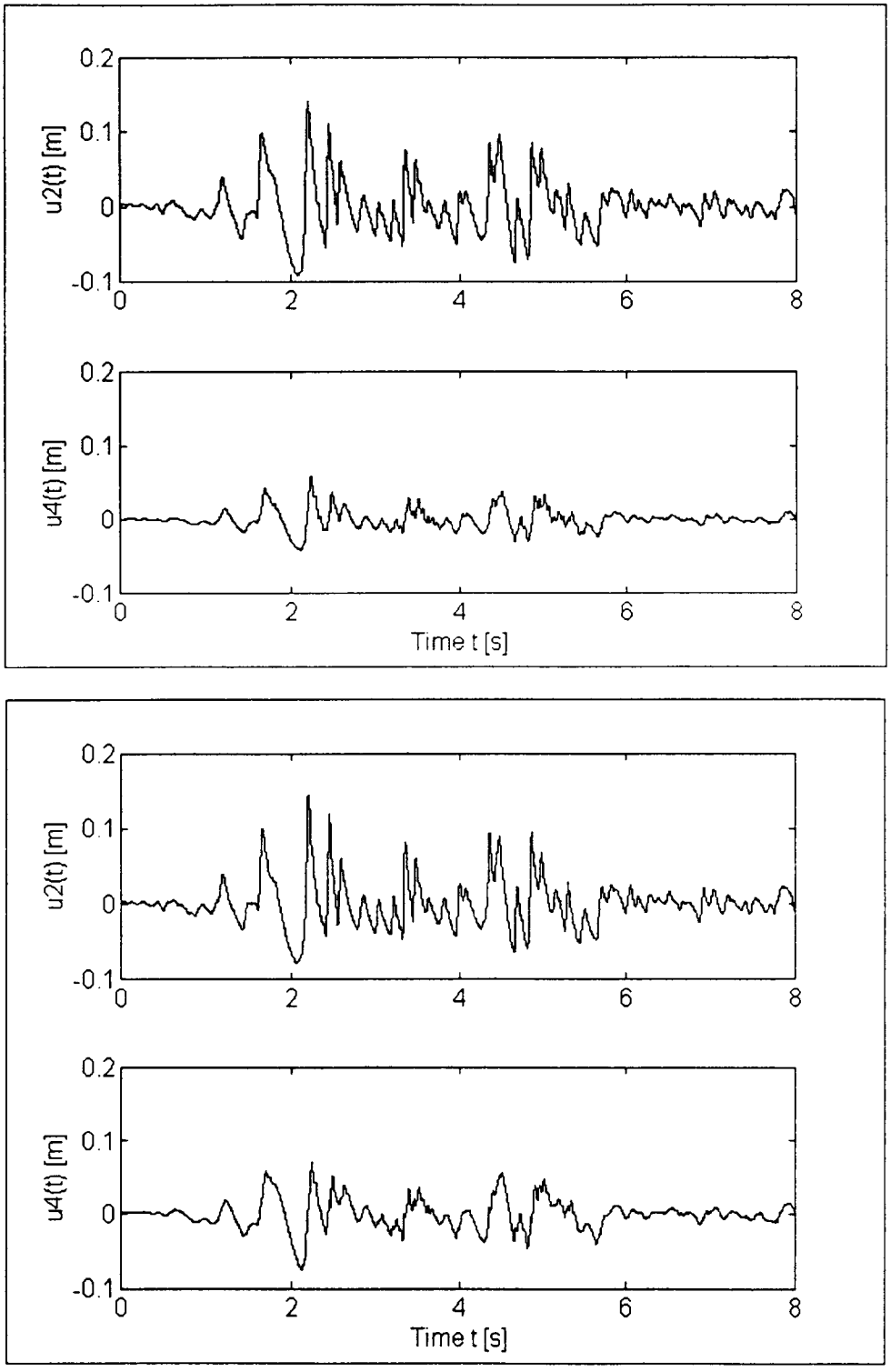

Figure 3.8: Control displacements of decentralized and global control

4. Discussion of Results

In this thesis it was shown that decentralized velocity feedback is capable of significantly reducing the vertical vibration of a two-cable-stayed beam structure under the influence of an external excitation. The resulting controllers are simple and easy to implement. No information needs to be transmitted along the beam structure since the sensors and actuators are collocated. The decentralized controllers have been designed based on a finite-dimensional lumped mass model of the beam structure. The control gains were chosen based on a generalized root locus plot and also as a result of applying optimal control to the decoupled subsystems. The performance of the decentralized control strategy was demonstrated by computer simulations. It was also shown that changes in the system parameters have only a minor effect on the system response. The decentralized control compares well to a global optimal control strategy.

The results of this work can be applied in the active control of cable-stayed bridges. There the linear properties of the beam model that was studied here are not necessarily valid. However, based on results of several researchers, the linear dynamic analysis of cable-stayed bridges is generally acceptable (26). Morris (27) also concludes that linear analysis results in a suitable description of the dynamic response of a cable-stayed bridge.

The effect of the stay cables as described by equation (2.5) is only valid if the actuator displacements and the vertical motion of the bridge deck are small compared to the static cable elongation. Sag of the stay cables is also a source of nonlinearities in the system. The problem of vibration of the stay cables was also investigated. It was

found in (28) that there is a significant effect of the stay cable vibration on the dynamic response of the system.

Another important issue in the application of the proposed active control is the performance of the actuators. Their power, maximum displacement, and dynamics will limit the control activity that is possible at any given time. This limitation leads most likely to a deterioration of the performance of the control system and has to be studied.

These are only some of the opportunities for further research in this field. In the future an active control system could become an integral part of cable-stayed bridges that is incorporated in the design from the beginning.

Bibliography

1. Lions, J. L. 1988. *Exact controllability, stabilization, and perturbations for distributed systems.* SIAM Review (ISSN 0036-1445), v30, pp. 1-68.

2. Yang, Jann N., and Fanis Giannopolous. 1979. *Active control and stability of cable-stayed bridge.* ASCE proceedings, Vol. 105, No. EM4, pp. 677-694.

3. Yang, Jann N., and Fanis Giannopolous. 1979. *Active control of two-cable-stayed bridge.* ASCE proceedings, Vol. 105, No. EM5, pp. 795-810.

4. Scheer, Dietmar. 1993. *Active robust control of cable-stayed bridges.* Master's thesis in electrical and computer engineering. Oregon State University.

5. Ohsumi, Akira and Yuichi Sawada. 1993. *Active control of flexible structures subject to distributed and seismic disturbances.* Journal of dynamic systems, measurement, and control, Vol. 115, pp. 649-657.

6. Tadjbakhsh, Iradj G., and Yuan-an Su. 1989. *Optimal, coupled-modal control of distributed parameter systems with discrete actuators.* Journal of applied mechanics, Vol. 56, pp. 941-946.

7. Morgan, Dennis R. 1991. *An adaptive modal-based active control system.* Journal of the acoustical society of America, Vol. 89, No. 1, pp. 248-256.

8. Meirovitch, L. 1987. *Some problems associated with the control of distributed structures.* Journal of optimization theory and applications, Vol. 54, No. 1, pp. 1-21.

9. Meirovitch, L., and L. M. Silverberg. 1983. *Globally optimal control of self-adjoint distributed systems.* Optimal control applications and methods, Vol. 4, pp. 365-386.

10. Meirovitch, L., and D. Ghosh. 1987. *Control of flutter in bridges.* Journal of engineering mechanics, Vol. 113, No. 5, pp. 720-736.

11. Balas, M. J. 1978. *Active control of flexible systems.* Journal of optimization theory and applications, Vol. 24, pp. 415-436.

12. Balas, Mark J. 1991. *Nonlinear finite-dimensional control of a class of nonlinear distributed parameter systems using residual mode filters: a proof of local exponential stability.* J. Math. Anal. Appl., Vol. 162, no. 1, pp. 63-70.

13. Balas, Mark J. 1988. *Finite-dimensional controllers for linear distributed parameter systems: exponential stability using residual mode filters.* J. Math. Anal. Appl., Vol. 133, no. 2, pp. 283-296.

14. Chen, Y. H. 1991. *Decentralized adaptive robust control design: The uncertainty is time varying.* Journal of dynamic systems, measurement, and control, Vol. 113, pp. 515-518.

15. Chen, Y. H. 1992. *Decentralized robust control for large-scale uncertain systems: A design based on the bound of uncertainty.* Journal of dynamic systems, measurement, and control, Vol. 114, pp. 1-9.

16. Šiljak, Dragoslav D. 1991. *Decentralized control of complex systems.* Mathematics in science and engineering, v. 184. San Diego: Academic Press, Inc.

17. Subcommittee on cable-stayed bridges of the committee on long-span steel bridges of the committee on metals of the structural division. 1977. *Bibliography and data on cable-stayed bridges.* ASCE proceedings, Vol. 103, No. ST10, pp. 1971-2004.

18. Warnitchai, Pennung, Yozo Fujino, Benito M. Pacheco, and Remi Agret. 1993. *An experimental study on active tendon control of cable-stayed bridges.* Earthquake engineering and structural dynamics, Vol. 22, pp. 93-111.

19. Roark, Raymond J. 1989. *Roark's formulas for stress and strain.* 6th edition. New York: McGraw-Hill.

20. Shabana, Ahmed A. 1991. *Theory of vibration.* Volume two: Discrete and continuous systems. New York: Springer-Verlag.

21. Garevski, Mihail A., and Roy T. Severn. 1993. *Damping and response measurement on a small-scale model of a cable-stayed bridge.* Earthquake engineering and structural dynamics, Vol. 22, pp. 13-29.

22. Wang, S. H., and E. J. Davison. 1973. *On the stabilization of decentralized control systems.* IEEE Trans. Automat. Control, Vol. 18, pp. 473-478.

23. Rosenbrock, H. H. 1974. *Computer-aided control system design.* London: Academic Press.

24. Ohta, Y., D. D. Šiljak, and T. Matsumoto. 1986. *Decentralized control using quasi-block diagonal dominance of transfer function matrices.* IEEE Trans. Automat. Control, Vol. AC-31, no. 5, pp. 420-429.

25. Anderson, Brian D. O., and John B. Moore. 1990. *Optimal control: Linear quadratic methods.* Englewood Cliffs: Prentice-Hall, Inc.

26. Wilson, John C. and Wayne Gravelle. 1991. *Modeling of a cable-stayed bridge for dynamic analysis.* Earthquake engineering and structural dynamics, Vol. 20, pp. 707-721.

27. Morris, Nicholas F. 1974. *Dynamic analysis of cable-stiffened structures.* ASCE proceedings, Vol. 100, No. ST5, pp. 971-981.

28. Abdel-Ghaffar, Ahmed M. and Magdi A. Khalifa. 1991. *Importance of cable vibration in dynamics of cable-stayed bridges.* Journal of engineering mechanics, Vol. 117, No. 11, pp. 2571-2589.

APPENDIX

Frequency Equation for Euler-Bernoulli Beam

Here the derivation of the structural frequency equation of the Euler-Bernoulli beam of Chapter 2.4 is performed. The expressions for the natural frequencies and the mode shapes directly follow from this derivation and are also repeated.

The free transverse vibration of an undamped Euler-Bernoulli beam is governed by the partial differential equation (20)

$$EI \frac{\partial^4 y}{\partial x^4} + m \frac{\partial^2 y}{\partial t^2} = 0 \qquad (A.1)$$

The solution to this equation can be obtained by using the technique of the separation of variables which assumes a solution of the following form:

$$y(x, t) = \beta(x) \cdot \alpha(t) \qquad (A.2)$$

Substitution of (A.2) into (A.1) yields the following general solution for $\beta(x)$ (20):

$$\beta(x) = D_1 \sinh \eta x + D_2 \cosh \eta x + D_3 \sin \eta x + D_4 \cos \eta x \ , \qquad (A.3)$$

where

$$\eta = \sqrt{\frac{\omega}{\sqrt{\frac{EI}{m}}}} \qquad (A.4)$$

The constants D_i (i=1,2,3,4) are determined by the boundary conditions of the beam. Here the beam is simply

supported at the left end and fixed at the right end. This defines the following boundary conditions:

$$y(0, t) = 0 \quad , \quad y''(0, t) = 0$$
$$y(L, t) = 0 \quad , \quad y'(L, t) = 0 \qquad (A.5)$$

The boundary conditions at the left end of the beam can be used to simplify equation (A.3) as follows:

$$y(0, t) = 0 \Rightarrow \beta(0) = 0$$

$$\beta(0) = D_2 + D_4$$

$$y''(0, t) = 0 \Rightarrow \beta''(0) = 0$$

$$\beta''(x) = \eta^2\left(D_1 \sinh \eta x + D_2 \cosh \eta x - D_3 \sin \eta x - D_4 \cos \eta x\right)$$

$$\beta''(0) = \eta^2\left(D_2 - D_4\right)$$

Assuming there are no rigid body modes (i.e., modes with a natural frequency of zero) this results in:

$$D_2 = D_4 = 0$$

and

$$\beta(x) = D_1 \sinh \eta x + D_3 \sin \eta x \qquad (A.6)$$

Next, the boundary conditions at the right end of the beam are used to determine D_1 and D_3:

$$y(L, t) = 0 \Rightarrow \beta(L) = 0$$

$$\beta(L) = D_1 \sinh \eta L + D_3 \sin \eta L$$

$$y'(L, t) = 0 \Rightarrow \beta'(L) = 0$$

$$\beta'(x) = \eta(D_1 \cosh \eta x + D_3 \cos \eta x)$$

$$\beta'(L) = \eta(D_1 \cosh \eta L + D_3 \cos \eta L)$$

or, in matrix form:

$$\begin{bmatrix} \sinh \eta L & \sin \eta L \\ \eta \cosh \eta L & \eta \cos \eta L \end{bmatrix} \begin{bmatrix} D_1 \\ D_3 \end{bmatrix} = \begin{bmatrix} 0 \\ 0 \end{bmatrix} \qquad (A.7)$$

For a non-trivial solution of (A.7) the determinant of the matrix has to be zero, i.e.,

$$\sinh \eta L \cdot \eta \cos \eta L - \sin \eta L \cdot \eta \cosh \eta L = 0$$

Division by $-\eta \cosh \eta L$ yields the frequency equation for the beam with the given boundary conditions:

$$\sin \eta L - \cos \eta L \cdot \tanh \eta L = 0$$

This equation has an infinite number of solutions η_i. The natural frequencies follow from (A.4):

$$\omega_i = (\eta_i L)^2 \cdot \sqrt{\frac{EI}{mL^4}} \quad , \quad i=1,2,\ldots$$

Finally, the mode shape associated with each natural frequency follows from equations (A.6) and (A.7). The solutions of the frequency equation make the two equations in (A.7) linearly dependent, so either one can be used. For example substitution of the first equation into (A.6) yields the following expression for the mode shapes:

$$\beta_i(x) = H_i\left[\sin \eta_i x - \frac{\sin \eta_i L}{\sinh \eta_i L} \sinh \eta_i x\right] \quad , \quad i = 1,2,\ldots \ ,$$

where the H_i's are arbitrary constants.